Automated data-processing technique: 2D Map for identifying the distribution of the U-value in building elements by quantitative internal thermography

Blanca Tejedor [a*], Eva Barreira [b], Ricardo M.S.F. Almeida[b,c], Miquel Casals[a]

[a] Universitat Politècnica de Catalunya (UPC). Department of Project and Construction Engineering. Group of Construction Research and Innovation (GRIC). C/ Colom, 11, Ed. TR5, 08222 Terrassa (Barcelona), Spain

[b] CONSTRUCT-LFC, University of Porto, Faculty of Engineering (FEUP), Civil Engineering Department, Rua Dr. Roberto Frias, 4200-465 Porto, Portugal

[c] Department of Civil Engineering, Polytechnic Institute of Viseu, Campus Politécnico, 3504-510 Viseu, Portugal

[*]Corresponding author: Blanca Tejedor. Tel: (+34) 93 7398919, E-mail: blanca.tejedor@upc.edu

Abstract

Computing a 2D colour map of average U-values pixel-by-pixel could become a challenging task in terms of complexity and time, especially for entire façades under the influence of anomalies. In a quantitative IRT test, a thermal image with a resolution of 320 x 240 pixels involves 76800 elements with different TWALL for each instant "t". This research aims to create a thermographic 2D U-value map for the characterization of heavy walls in a stationary regime. The method was divided into three steps: (i) metrology; (ii) assessment of how mesh discretization affects the image quality by MATLAB; (iii) development of a 2D map by SURFER. The results demonstrated that all 2D maps were a great reproduction of the original image, considering as optimum a TWALL mesh comprised of 1600 elements of 8x6 pixels. The automated data-processing method only took 20 minutes and image quality losses were estimated at 6.65%.

Keywords: quantitative infrared thermography, automated data-processing technique, measured U-value, processed image, 2D map, 2D correlation coefficient, quality image, MATLAB, SURFER

1. INTRODUCTION

The building envelope is often considered the largest surface area in contact with the external environment [Adhikari et al., 2012; Bienvenido-Huertas et al., 2019]. Along this line, several authors have stated that walls have a greater impact on the energy demand of a building than other construction elements [Dowson et al., 2012; Battista et al., 2014; Kurtz et al., 2015; Mortarotti et al., 2017; Park et al., 2017]. In the last decades, the thermal transmittance has become a key parameter for evaluating the built quality and steady-state heat transmission performance [Ferrari et al., 2013; Nardi et al., 2014; Soares et al., 2019]. Hence, an accurate U-value is crucial to: (i) optimize the design of buildings [Soares et al., 2019]; (ii) evaluate thermal comfort and estimate the energy requirements (heating, ventilation and air conditioning systems) and the energy savings in the operational stage [Peng et al., 2008; Melo et al., 2015; Garrido et al., 2018; Bienvenido-Huertas et al., 2019; Soares et al., 2019]; (iii) protect the built cultural heritage [Avedilidis et al., 2000; Moropoulou et al., 2013; Soares et al., 2019]; (iv) support decision making for the maintenance or refurbishment of existing buildings comprised of non-homogeneous assembled materials (often degraded over time and with unknown properties) [Stimolo et al., 2003; Bashkar et al., 2006; Sassine et al., 2016; Tejedor et al., 2018]. However, the U-value may be modified by anomalies, which are sometimes invisible, leading to incorrect adoption of calculation procedures or management strategies for the above purposes. Indeed, not all European countries consider the impact of thermal bridges in their respective standards for new buildings and for the refurbishment of the existing ones [Dumitrescu et al., 2016]. Aspects such as ageing and morphology of the specimen, local hygrothermal data or building pathologies are often neglected in regulatory calculation procedures (i.e. ISO 6946) [Doran, 2001; Baker, 2013; Lucchi, 2017; Genova et al., 2018]. For this reason, conventional onsite monitoring systems are essential for a construction project [Park et al., 2016; Kropp et al., 2018]. Despite this, the inspection of building elements often depends on manual processes [Garrido et al., 2018a] and vision-based recognition methods do not deal with interior sites [Kropp et al., 2018]. To overcome these limitations, quantitative infrared thermography (QIRT) can be implemented as an alternative non-destructive testing (NDT) for measuring the in-situ U-value. Nevertheless, methodologies to automate the analysis of thermal transmittance pixel-by-pixel are still in progress [Asdrubali et al., 2012; Nardi et al., 2018]. Hence, this paper proposes an automated data-processing technique to create a 2D U-value map of walls with pathologies based on internal QIRT. A summary of existing approaches about diagnosis of pathologies in façades and automation of thermographic evaluations is given in Section 2.

2. BACKGROUND

2.1. Diagnosis of pathologies in façades by thermography

In recent years, some authors have developed strategies to identify and assess anomalies in façades, especially those affected by ageing [Cereijo et al., 2014; Edis et al., 2015; Cadelano et al., 2015; Georgescu et al., 2017; Lucchi et al., 2017; Asdrubali et al., 2018; Martínez-Garrido et al., 2018; Garrido et al., 2018a; Garrido et al., 2018b; Garrido et al., 2019a; Garrido et al., 2019b; Ruiz Valero et al., 2019]. Martínez-Garrido et al. [2018] and Ruiz Valero et al. [2019] used SURFER [Golden Software, 2018] to map the distribution of moisture content in historic building envelopes. Rough estimations of the extent of damp problems were obtained by combining various NDT (i.e. qualitative IRT) with the readings of Electrical Conductivity Meter (EC) or Electrical Resistance Measuring (ERM). Subsequently, the most intense fronts were characterized by Electrical Resistivity Tomography (ERT) and Ground Penetrating Radar (GPR) for better identification of the source of the anomaly. It should be noted that the interpretation of the outcomes of Moisture Mapping (MM) was mainly geometrical (homogeneity reading) and qualitative (resistivity vs. moisture) in both studies. Furthermore, some limitations were mentioned in previous studies. For example, moisture content readings could differ significantly due to the use of a variety of meters in the same operating conditions [William, 1997; Jukka, 2005] and a single measurement point may not be enough representative of the status of the entire structure [Göller, 2013].

Regarding thermal bridges, there is a lack of reliable and simple methodologies for diagnosing entire walls affected by defects. Indeed, some studies have computed psi-values (also termed linear thermal transmittance) to quantify the impact of anomalies on façades using a line-meter in the thermographic analysis or applying simulation tools based on finite elements and fluid dynamics (THERM, FLUENT and GAMBIT among others) [Asdrubali et al., 2012; Martin et al., 2012; Nardi et al., 2015; O'Grady et al., 2017; Baldinelli et al., 2018; O'Grady et al., 2018; Sfarra et al.,2019]. One of the limitations of algorithms based on the line segment extraction is the creation of descriptors and their dependency on the line length [Zhang et al., 2013; Zhao et al., 2016; Kropp et al., 2018]. The measured thermo-physical property is linked to the wall surface temperature of each pixel that comprises the line segment created by the researchers [Asdrubali et al., 2012]. In other words, a single line segment is evaluated as a representative part of the effect of the pathology on the entire wall. Hence, the extension of the area of the pixel depends from the IFOV of the IR camera [Asdrubali et al., 2012]. Besides this, the algorithm implementation and the high

computation time of 3D models are often considered a disadvantage by not specialized researchers (i.e. energy auditors) [Gao et al., 2004; Sala, 2008; Lucchi et al., 2017; Lucchi et al., 2018]. Complex models are characterized to require detailed input data on meteorological observations, stratigraphy, order of the material layer, and features of each material layer (i.e. thickness, conductivity, density, thermal mass, vapour pressure resistance, emissivity and risk of surface condensation) [Wróbel et al., 2008; Lehman et al., 2013; Lucchi et al., 2017; Nardi et al., 2018]. Concerning the IRT analysis, the interpretation of the thermograms is conducted by a human operator in both building pathologies (thermal bridges and moisture). The knowledge of the geometry, temperature distribution and test conditions are needed for a correct identification of the anomaly [Garrido et al., 2018a]. However, the assessment depends on the subjectivity and expertise of the technician [Garrido et al., 2018a; Garrido et al.,2019a]. Indeed, Hiasa et al. [2017] affirmed that processing data mathematically could lead to increase the objectivity in the diagnosis of defects in civil structures. Nevertheless, the automation of the analysis of U-value pixel-by-pixel is still ongoing [Asdrubali et al., 2012; Nardi et al., 2018].

2.2. Automation of the thermographic analysis pixel-by-pixel under stationary regime

The development of a 2D colour map of average U-values could be challenging due to the complexity and time required. Calculation procedures based on QIRT from inside or outside the building are complex [Hoyano et al., 1999; Madding et al., 2008; Albatici et al., 2010; Fokaides et al., 2011; Dall'O et al., 2013; Liu et al., 2015; Nardi et al., 2016; Tejedor et al., 2017]. Indeed, previous studies highlighted some shortcomings that arise in the external QIRT in terms of susceptibility of the outdoor environmental conditions, control of reflection index of objects with unknown thermal status, overestimation of the convective heat transfer coefficient and effect of the wind speed in the calculation procedure [Hoyano et al., 1999; Emmel et al., 2007; Palyvos et al., 2008; Fokaides et al., 2011; Rabadiya et al., 2012; Sham et al., 2012; Dall'O et al., 2013; Liu et al., 2015; Tejedor et al.; 2017]. To avoid the issues mentioned above, the internal QIRT may be adopted for creating a 2D U-value map. Instantaneous U-values ($U_{QIRT\ ins}$) are expressed as a function that involves convection and radiation heat transfer processes in a stationary regime. Once all the measurements have been calculated for a total of "N" thermograms, the average measured U-value ($U_{QIRTavg}$) is defined. Notably, some parameters of the existing numerical models can be assumed to be constant during the calculation procedure: Stefan-Boltzmann's constant (σ), air thermal conductivity (λ_{air}), wall surface emissivity (ε_{WALL}), wall height (L) or even the Rayleigh (R_a) and Prandtl (P_r) numbers in

the dimensionless approaches. Other parameters such as the reflected ambient temperature (T_{REF}) and air environment temperatures (T_{IN} and T_{OUT}) can be incorporated for each instant, regardless the wall area to be analyzed. In contrast, the wall surface temperature (T_{WALL}) may compromise a lower or higher number of pixels to be processed depending on whether or not the building element has enough heat flux homogeneity due to an anomaly. In terms of time consumption, the common technical specifications of an IR camera establish that a thermal image with dimensions 320 x 240 pixels is composed of 76800 elements (1 x 1 pixel), which involves a width/height ratio of 1.33. Tejedor et al. [2019] stated that the usual approach adopted for QIRT could imply manual post-processing from 120 to 7200 thermograms with data acquisition intervals of 1 min to 1 s respectively. Therefore, 76800 elements with different T_{WALL} should be computed for each instant "t" to generate a 2D U-value map. Consequently, the simplification of the calculation procedure should be considered, with larger boxes or elements of average T_{WALL} to work with a simpler processed image. Nevertheless, the methodologies to automate the thermographic analysis pixel-by-pixel are still in development [Asdrubali et al., 2012; Nardi et al., 2018].

The literature review revealed few automated NDT approaches under a stationary regime for the construction industry field. Brilakis et al. [2011] and Park et al. [2016] applied vision-based tracking methods to improve the control of the outdoor construction activities on dynamic state and to automate the on-site progress monitoring. Kropp et al. [2018] focalized their study on the automation of interior construction state recognition using registered images and a 4D BIM model. Video frames were captured with a monocular camera system during the inspection. Subsequently, the building model was superimposed onto the image in an augmented reality, conducting different steps of image registration (i.e. line segment extraction, fine pose estimation, rough motion estimation etc) and image recognition (i.e. space reduction and image rectification among others). Montanini et al. [2016], Chrysafi et al. [2017] and D'Accardi et al. [2018] developed algorithms to process thermograms under transient conditions for manufacturing processes, to enhance the readability of images. In some studies, related to bioinformatics applications or NDT for measuring material deformation, the pattern recognition and image processing methods were mainly focused on the 2D correlation coefficient [Kaur et al., 2012; Blaber et al., 2015; Mohapatra et al., 2018]. Pearson's correlation coefficient (R) is one of the most commonly used statistical tool to determine the linear correlation degree in pixel-by-pixel intensity between two data sets **A** and **B** [Mohapatra et al., 2018]. To achieve this, both images should be assumed to be arrays, where **A** refers to

the original image and **B** is a simpler processed image. Although it is computationally intensive, the dimensionless index *R* is a single scalar value that is invariant to linear transformations and insensitive to variations in brightness or contrast across the image [Kaur et al., 2012]. Hiasa et al. [2017], Sultan et al. [2017] and Milovavic [2019] detected pixel-by-pixel surface delamination in concrete bridge decks and other concrete structures by means of active IRT, finite elements and the statistical tool PCA (Principal Component Analysis). Only some Spanish and Italian studies adapted the existing visible image processing techniques to automate the identification of pathologies in walls by IRT [González-Jorge et al., 2012; Cereijo et al., 2014; Asdrubali et al., 2018; Garrido et al., 2018a; Garrido et al., 2018b; Garrido et al., 2019a; Garrido et al., 2019b]. Garrido et al. [2018a] proposed an improvement of Cereijo's approach, reducing the number of false thermal bridges detected from outside the building through the computation of the linear thermal transmittance and increasing the accuracy by an image rectification procedure based on geometrical characterization. The implementation of the photogrammetric technique was used as a map for the characterization of a thermal bridge in terms of width or height. It should be noted that the image rectification process (horizontal and vertical direction) was necessary to correct the sum of distortions (projection, perspective and radial) caused by the lens of a IR camera hitched to a mobile inspection vehicle. Garrido et al. [2018b] used two thermal criteria and PCT (Principal Component Thermography) method to process raw data in order to detect and classify 3 thermal bridges and 3 areas with moisture. The thermograms were acquired from internal and external surfaces of building envelopes. This study was focused on qualitatively assessing the temperature distribution of each transition phase between each defect and its undisturbed surroundings. A pre-processing and a post-processing steps were required, specifically to eliminate the noise of the image and to extract the geometrical boundaries of the anomaly. Along this line, Garrido et al. [2019a] implemented three techniques of image post-processing: thresholding, bilateral filtering and findContours to external walls with moisture. The main goal was to increase the difference in pixels between the moisture areas and undisturbed areas, to remove the existing noise in the image and to implement a geometric and a thermal filter. The authors also stated that the temperature distribution of a thermogram could be assumed as pseudo-bimodal distribution with two Gaussian bells combined. Garrido et al. [2019b] presented some algorithms to automatically detect and characterize heritage structures with moisture from outside the building. The methodology was also focused on two thermal criteria and a semi-automatic image rectification process. Skewness and kurtosis values were checked to determine moisture candidate regions.

2.3. Problem statement and research objectives

As described earlier, the determination of an accurate U-value is an essential in terms of built quality and energy savings. However, the analysis pixel-by-pixel of an entire façade with pathologies has become a challenging task for the building inspection, especially in steady-state conditions. The extensive literature review shows that: (i) the diagnosis of pathologies is mainly qualitative; (ii) calculation procedures are complex and time consuming; (iii) a thermographic mapping of the façade often requires the use of complementary approaches to determine the thermal transmittance (i.e. complex CFD models in transient regime, a set of image processing techniques or additional measurement methods -ERT, GPR, EC-); (iv) a line segment is adopted as a representative part of the effect of the pathology. Furthermore, the most advanced methods only provide a processed image of the construction material in grayscale with the real contours of the existing anomalies in red lines.

To solve these problems, the current paper aims to create a 2D U-value map based on quantitative internal IRT under stationary regime. Assuming the thermal image as a temperature matrix, and according to the background, the decision criterion of the proposal should be focused on the 2D correlation coefficient. In this way, it could be possible to work with a simpler processed thermogram and observe easily the associated dispersions of the measured U-value under the influence of pathologies, along vertical and horizontal axes of the building element. Within this context, the conceptual framework of the paper addresses the specific research objectives that are presented below. Firstly, the impact of mesh discretization in the quality of the thermal image was evaluated by means of MATLAB [Mathworks, 2018]. Secondly, a 2D colour map was developed using SURFER [Golden Software, 2018]. To demonstrate the applicability of the proposed innovative technique, three common constructive solutions in Southern European countries were selected and assessed by QIRT method reported in Tejedor et al. [2017]. Subsequently, the reliability and quality of the process was checked through an alternative NDT such as HFM (Heat Flux Meter), applying ISO 9869-1:2014 [International Organization for Standardization, 2014]. Notably, performance metrics of the detection system (recall, precision and F-score) were not determined, since image recognition and rectification techniques were not applied.

3. DEVELOPMENT OF THE METHOD

The method, which is represented in Figure 1, is fully described in Sections 3.1 (Metrology: Non-destructive testing and materials), 3.2. (Influence of mesh discretization on the quality of the processed image) and 3.3. (Development of a U-value map).

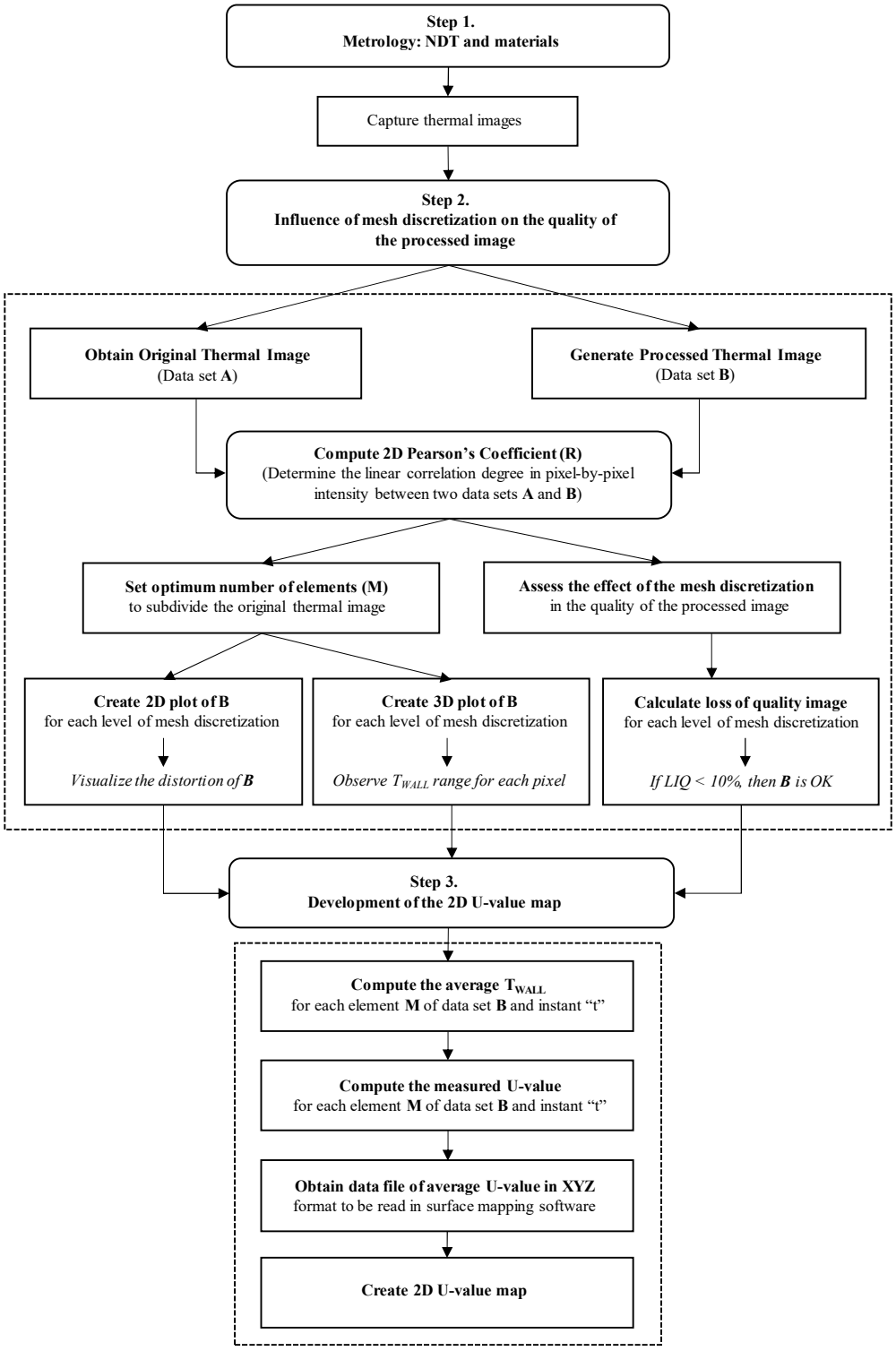

Figure 1. Flowchart of the proposed method

3.1. Metrology: Non-destructive testing (NDT) and materials

Laboratory testing for the thermal characterization of homogenous and non-homogeneous building structures or composite assemblies under steady-state conditions is considered one of the diagnosis techniques that has the lowest measurement errors, since it does not depend on climate conditions [Chen et al., 2012; Soares et al., 2019]. Thus, measurements were conducted in a walk-in climatic chamber (FITOCLIMA 1000, EDTU) of the Laboratory of Building Physics of FEUP (Faculty of Engineering of the University of Porto), as seen in Figure 2.

Figure 2. Inside and outside the climatic chamber of FEUP

To implement QIRT by the methodology proposed by Tejedor [2017], the walls were pre-conditioned in the climatic chamber. In this way, a stable temperature gradient and homogeneity of the heat flux were ensured. Taking into account that the T_{OUT} and RH_{OUT} were by default 18 -20ºC and 40% respectively, the inner environmental parameters were configured to be T_{IN}= 35ºC and RH=50% before and during the tests. As regards the measuring equipment, an IR camera (NEC TH9100MR) and aluminum crinkled foil were positioned inside the metering box, to monitor the wall surface temperature (T_{WALL}) and the reflected ambient temperature (T_{REF}). This IR camera was characterized to present a temperature range from -20ºC to 100ºC, a resolution of 320 x 240 pixels and an accuracy of ±2% reading. In addition, inner and outer air ambient temperature were collected by two encapsulated temperature sensors and data loggers (HOBO UX100), with a resolution of 0.024ºC and an accuracy of ±0.21ºC. The wall surface emissivity (ε_{WALL}) was determined with an emissometer (D&S Model AE1), obtaining a value of 0.93 for all walls. All the IRT tests only took 2h and the data acquisition interval was set to 1 minute, so that a total of 120 thermograms were captured. To perform the HFM method for subsequent validation of 2D maps, two transducers and data loggers (TPD TND-TH PU3.2) with an accuracy of ±5 were added to the experimental procedure. Data

were recorded for 72h with a sampling frequency of 10 minutes, following ISO 9869-1:2014 recommendations [International Organization for Standardization, 2014].

Concerning case studies, three heavy walls were chosen as representative samples of Southern European constructions. Different kinds of anomalies were built to alter the external or internal configuration of the wall, to observe variations in the thermal behavior of the wall and to check the limitations and potentials of the proposed automated data-processing technique. W1 consisted of a single-leaf wall of 0.25 m of lightweight concrete. The specific characteristic of this sample was the existence of air voids in the internal structure of the brick that could have affected the thermal behavior of the building component. W2 was a heavy multi-leaf wall that had superficial thermal bridges (0.06 x 0.06 m^2) of different depths (0.025 m, 0.050 m and 0.065 m). The internal configuration of this wall (from the outside to the inside) was: 0.25 m of lightweight concrete, 0.01 m of lightweight mortar, 0.065 m of projected thermal plaster, 0.005 m of bonding mortar with fiberglass and 0.010 m of mineral mortar. W3 was a heavyweight multi-leaf wall with 0.250 m of lightweight concrete, 0.010 m of lightweight mortar, 0.060 m of EPS and 0.005 m of plasterboard. In this case study, the main feature was a large internal horizontal thermal bridge (0.88 x 0.20 m^2). The composition of the three walls is shown in Figure 3 by means of a schematic section. Notably, the metering box was sufficiently large to evaluate full-scale components of 1.9 m height.

Fig. 3 (a). Single-leaf wall with internal air voids (W1)

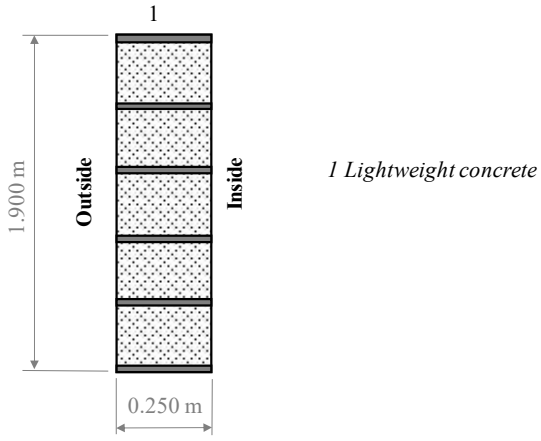

Fig. 3 (b). Multi-leaf wall with superficial thermal bridges (W2)

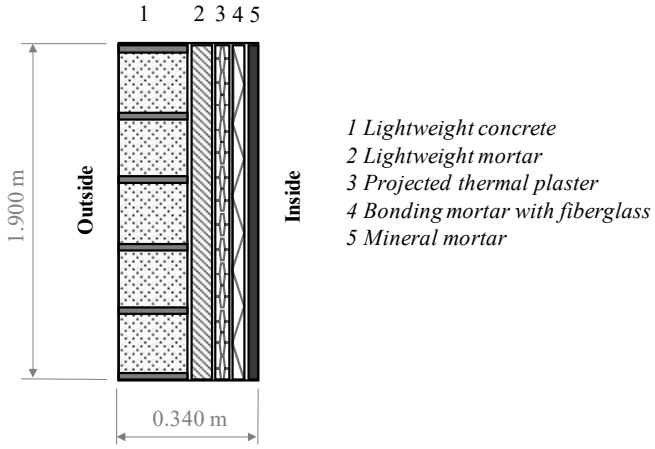

Fig. 3 (c). Multi-leaf wall with internal horizontal thermal bridge (W3)

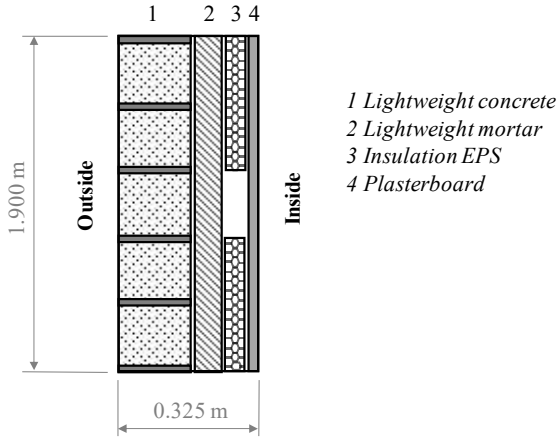

261

262 Figure 3. Schematic section of the walls. (a) Single-leaf wall with internal air voids (W1); (b) Multi-leaf

263 wall with superficial thermal bridges (W2); (c) Multi-leaf wall with internal horizontal TB (W3)

264

3.2. Influence of mesh discretization on the quality of the processed image

Before a 2D U-value map is created, the features of the processed image needed to be defined to achieve a reliable automated tool. Therefore, this section was divided into two steps. The first one was to determine the optimum number of elements to subdivide the original thermal image (**A**). The second step was to assess the effect of mesh discretization on the quality of the processed image (**B**) that will be used later to develop the 2D U-value map.

Taking into account the aspects mentioned in the literature review, Pearson's correlation coefficient (R) was computed between the original thermogram (**A)** and the same processed image (**B**), as defined in Equation 1:

$$R = \frac{\sum_{i=1}^{j}\sum_{j=1}^{i}(A_{ij}-\bar{A})\cdot(B_{ij}-\bar{B})}{\sqrt{\sum_{i=1}^{j}\sum_{j=1}^{i}(A_{ij}-\bar{A})^2}\cdot\sqrt{\sum_{i=1}^{j}\sum_{j=1}^{i}(B_{ij}-\bar{B})^2}} \quad (1)$$

Where *i* and *j* are the number of rows and columns in the image arrays. A_{ij} and B_{ij} are the intensities of pixel *ij* from the data sets **A** and **B**. $\bar{A}$ and $\bar{B}$ can be defined as the mean pixel intensities of data sets **A** and **B**. Notably, array **B** was defined for different levels of discretization (Table 1), but the width/height ratio of the reference thermogram was always maintained. For example, if **B** was divided into 1600 elements, the thermal image contained 40x40 elements of *8x6* pixels each one and 1.33 of width/height ratio. Then, the average wall surface temperature (T_{WALL}) was calculated for each one of these elements, leading to the same value for 8 pixels in horizontal and for 6 pixels in vertical.

Table 1. Levels of discretization and n-elements to subdivide the thermal image

Levels of discretization (Number of Pixels for each element in array B)	**Width/Height ratio**	**M (Number of total elements to subdivide the image)**
8 x 6	1,333	1600 (40 x 40)
16 x 12	1,333	400 (20 x 20)
32 x 24	1,333	100 (10 x 10)
64 x 48	1,333	25 (5 x 5)
160 x 120	1,333	4 (2 x 2)

The measure of similarity between images did not consider luminance, contrast and structure during the quality assessment, in comparison with other image recognition studies. The main reason is that these three parameters were the same in all cases. Neither the "aliasing" filter was applied, since the resolution of data sets **A** and **B** was the same (320 x 240 pixels) and the only variant factor was the number of elements.

After calculation of the 2D correlation coefficient, the mesh for each level of discretization was plotted in 3D and 2D by MATLAB [Mathworks, 2018]. The 3D graph allowed the observation of average T_{WALL} values for each pixel in array **B** with dimensions 320 x 240 pixels, while the 2D graph clearly highlighted the distortion of processed image **B**. To assess the effect of level discretization, the loss of image quality (LIQ) was calculated by Equation 2 and plotted against the number of elements to subdivide the thermal image.

$$LIQ = (1 - R^2) \cdot 100 \quad (2)$$

If R was close to 1, this indicated that the loss of information was minimum (LIQ < 10%) when pixel intensities Aij and Bij were compared (data sets **A** and **B** were linearly correlated images). If R was equal or close to 0, then the impact of level discretization was significant and the quality of the processed image **B** was not representative enough to create a 2D U-value map.

3.3. Development of the 2D U-value map

When QIRT tests had been completed and the optimum number of elements had been determined to subdivide the thermal image (1600 of 8x6 pixels), the next step in the method was to develop the 2D colour map to identify the distribution of the thermal transmittance throughout the entire wall area under stationary regime.

For this purpose, a computer program was developed to automate the computation of the processed image (**B**) with average T_{WALL} values and subsequently, to obtain the average thermal transmittance of each element of the array through the formulation extensively reported in Tejedor et al., [2017] and briefly shown in Equations 3 and 4.

$$U_{QIRT_{ins}}\left[\frac{W}{m^2 \cdot K}\right] = \frac{\left\{0.825 + \frac{0.387 \cdot R_a^{\frac{1}{6}}}{\left[1+\left(\frac{0.492}{P_r}\right)^{\frac{9}{16}}\right]^{\frac{8}{27}}}\right\}^2 \cdot \lambda_{air}}{L} \cdot \frac{[T_{IN} - T_{WALL}] + \varepsilon_{WALL} \cdot \sigma \cdot [T_{REF}{}^4 - T_{WALL}{}^4]}{(T_{IN} - T_{OUT})} \quad (3)$$

$$U_{QIRT_{avg}}\left[\frac{W}{m^2 \cdot K}\right] = \frac{\sum_{t=1}^{N}(q_{r_i} + q_{c_i})}{\sum_{t=1}^{N}(T_{IN_i} - T_{OUT_i})} = \frac{\sum_{i=1}^{n} U_{QIRT_{ins}}}{N} \quad (4)$$

The output was a data file in XYZ coordinate format to be read by SURFER [Golden Software, 2018]. With the contouring and 3D surface mapping software, 2D U-value maps could be generated with the same scale of colours as a thermogram. To check the reliability of the process, all maps were compared with the local measurements provided by HFM tests according to Section 3.1. It should be noted that the formulation of the measured U-value had already been validated in several Spanish residential buildings with different features [Tejedor et al., 2017; Tejedor et al., 2018; Tejedor et al., 2019]. Considering that the laboratory of Building Physics of FEUP allowed to test the specimens in controlled environmental conditions, possible computation errors in the development of the U-value map could be easily detected.

4. DISCUSSION OF RESULTS

4.1. Influence of mesh discretization on the quality of the processed image

This section is designed to discuss how mesh discretization of the thermal image could influence the quality of outcomes in the second stage of the proposed automated data-processing method, the generation of the processed image B. By way of example, and according to Section 3.2, the results of 2D correlation coefficients with different levels of discretization for sample W1 are presented in Figures 4 and 5. At the outset, the original thermogram (A) is shown with its respective 3D plot by MATLAB, to see where the temperature peaks were produced. Afterwards, the same structure was used to visually analyse the evolution of the processed image (B) with lower levels of discretization (8x6 pixels, 16x12 pixels, 32x24 pixels, 64x48 pixels and 160x120 pixels). In contrast to other studies [Garrido et al., 2018b], this research did not pretend to obtain the acquisition of the contour of each anomaly by means of the PCT method and additional criterions, since PCT is normally applied in active IRT and their PCs (Principal Components) partially describe the temperature changes of pixels over time.

As can be observed, 3D and 2D plots presented an evident distortion along the variations in data set **B**. The range of the average wall temperatures was greater for high levels of mesh discretization (3D plots of Figures 4 and 5). In the case of the reference image (**A**), the scale of T_{WALL} was from 26 to 34ºC. For levels of discretization of 4 elements (where each one contains 160 x 120 pixels), the scale of T_{WALL} for array **B** was found to be between 30.4 and 31ºC. In fact, and in terms of the 2D correlation coefficient, R was equal to 0.287, which means that only 8.23% of the processed thermal image **B** can be attributed to the original thermogram **A**. Therefore, the loss of information in data set **B** could strongly affect in the development and accuracy of transmittance mapping. Besides this, an alteration in T_{WALL} distribution was detected for arrays with < 400 elements (2D plots of Figures 4 and 5). In terms of applicability for the future 2D U-value map, this aspect could make it harder for technicians to define the proportions of brick and mortar, the borders of the aluminium crinkled foil that should be avoided during the analysis of QIRT and so on.

Fig. 4 (a). Original Thermal Image (76800 elements with different average T_{WALL})

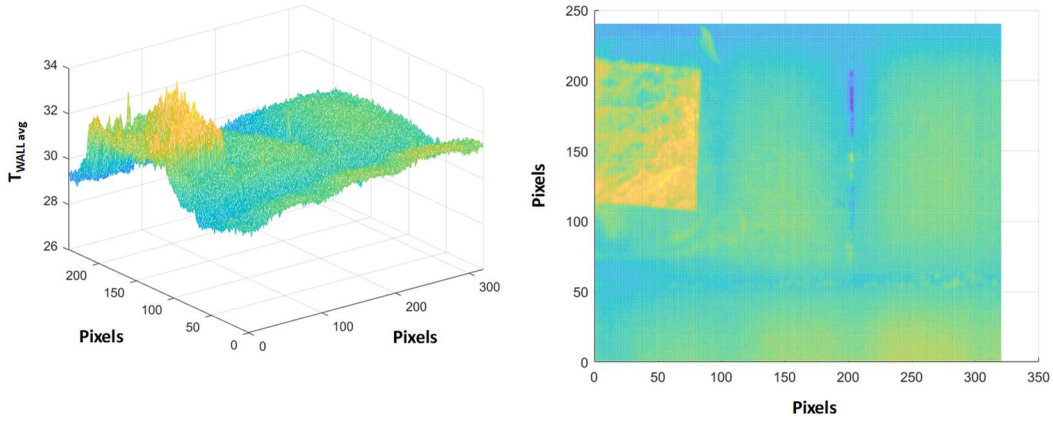

Fig. 4 (b). 8 x 6 pixels (1600 elements with different average T_{WALL})
2D Correlation Coefficient = 0.966

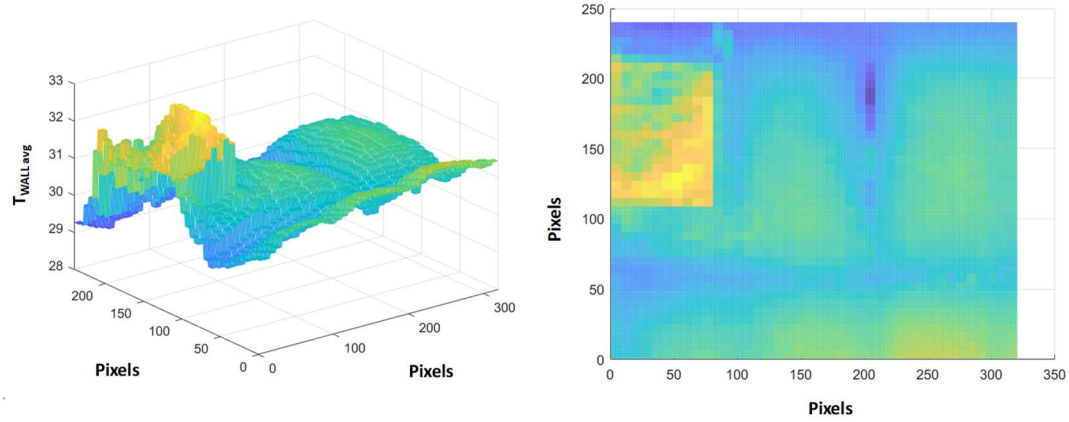

Fig. 4 (c). 16 x 12 pixels (400 elements with different average T_{WALL})
2D Correlation Coefficient = 0.945

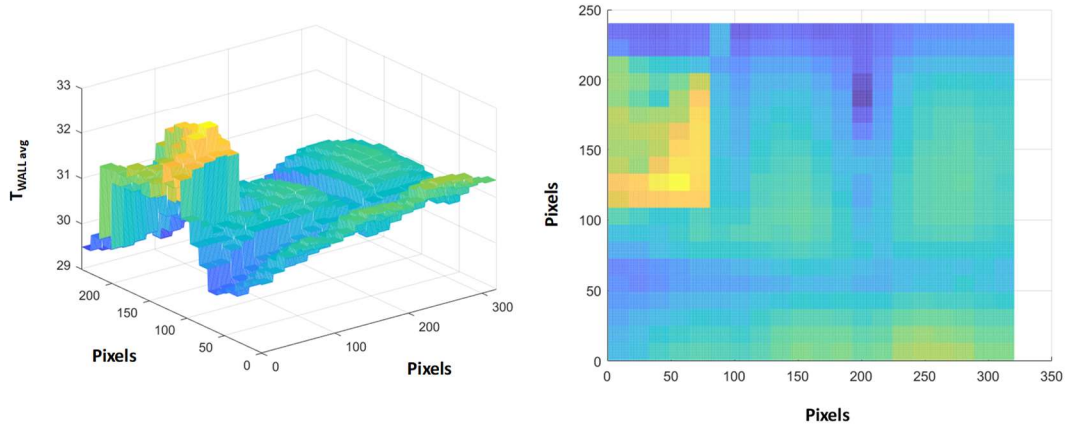

Figure 4. Determination of 2D Correlation Coefficient for different levels of discretization I. (a) Original thermogram; (b) Processed image with a mesh discretization of 8x6 pixels; (c) Processed image with a mesh discretization of 16 x12 pixels

Fig. 5 (a). 32 x 24 pixels (100 elements with different average T_{WALL})
2D Correlation Coefficient = 0.876

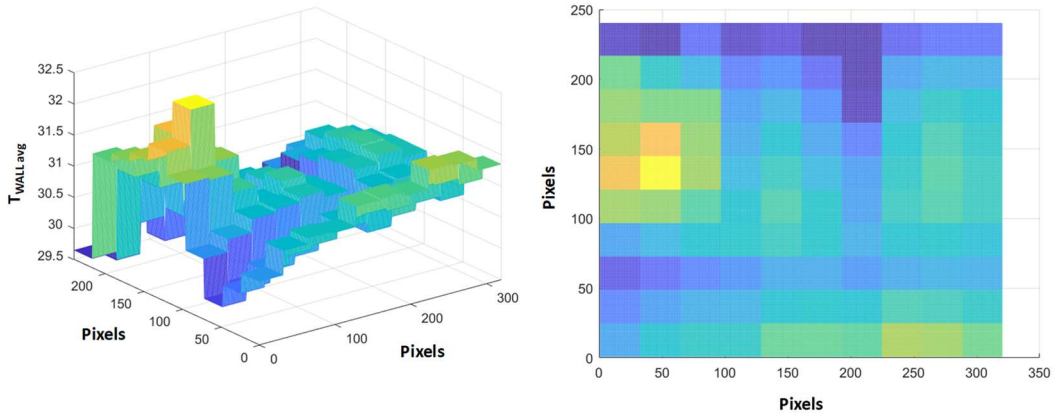

Fig. 5 (b) 64 x 48 pixels (25 elements with different average T_{WALL})
2D Correlation Coefficient = 0.717

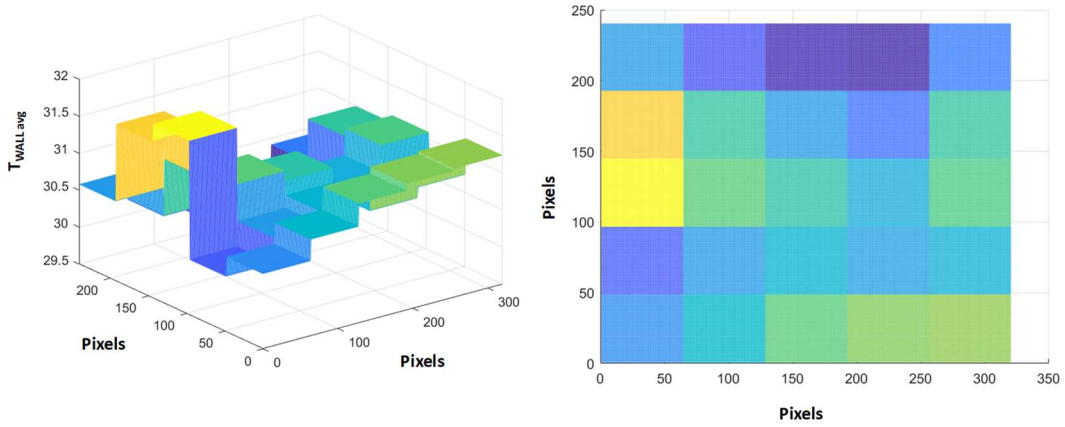

Fig. 5 (c). 160 x 120 pixels (4 elements with different average T_{WALL})
2D Correlation Coefficient = 0.287

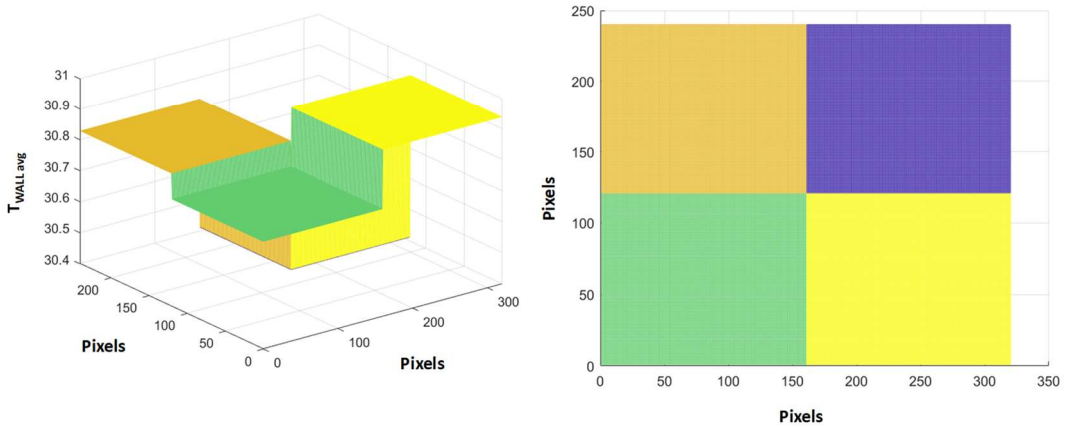

Figure 5. Determination of 2D Correlation Coefficient for different levels of discretization II. (a) Processed image with a mesh discretization of 32x24 pixels; (b) Processed image with a mesh discretization of 64x48 pixels; (c) Processed image with a mesh discretization of 160 x120 pixels

The parameter of assessment and quantification of image quality for data set **B** potentially decreased as levels of discretization were greater (Figure 6). Indeed, it could be drawn a curve defined by Equation 5.

$$LIQ = 186.26 \cdot M^{-0.457} \quad (5)$$

Where *LIQ* is the loss of image quality in [%] and *M* is referred to as the number of elements to subdivide the thermal image. This could help to determine the *LIQ* in future studies, without the need to calculate and plot a new data set **B**. In addition, this analysis corroborated the results of Figures 4 – 5 and demonstrated that the optimum number of elements in which to subdivide a thermogram should be 1600 (40 x 40 elements of 8x6 pixels each one), giving only 6.65% of *LIQ*.

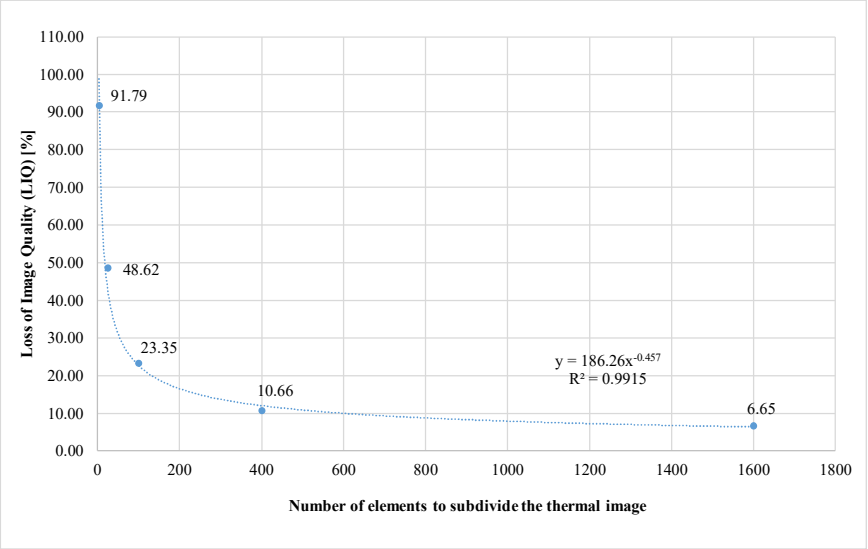

Figure 6. Impact of mesh discretization in the quality of the processed image (**B**).

4.2. Reliability and quality of the automated process

Three heavy walls were tested in a climatic chamber by quantitative infrared thermography (QIRT) and heat flux meter (HFM) under steady- state conditions. Figures 7 – 9 show the 2D U-value maps that were computed by SURFER [Golden Software, 2018], following the procedures explained in Sections 3.2. and 3.3. In the interpretation of these maps, it is important to note that the blue colour corresponds to cold spots with greater disturbance of the reference value and red spots refer to warmer areas. In addition, the areas of the aluminium crinkled foil were indicated with a discontinuous line in the IR images (temperature pattern) and 2D U-value maps.

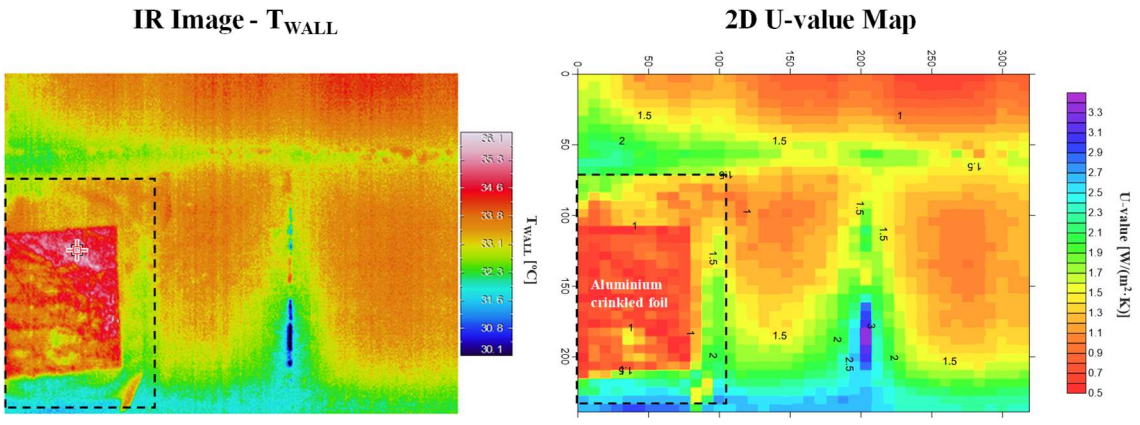

Figure 7. IR Image and 2D U-value map for the single-leaf wall (W1)

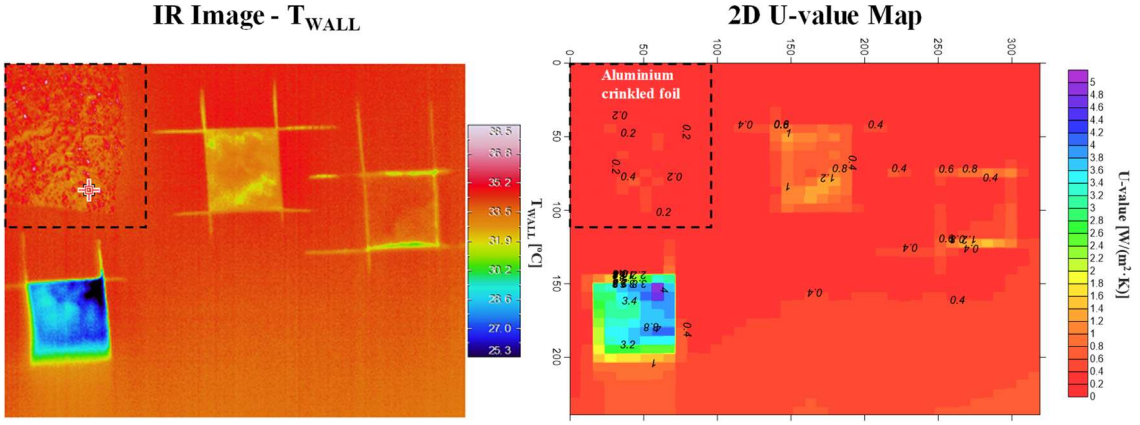

Figure 8. IR Image and U-value map for the multi-leaf wall with superficial thermal bridges (W2)

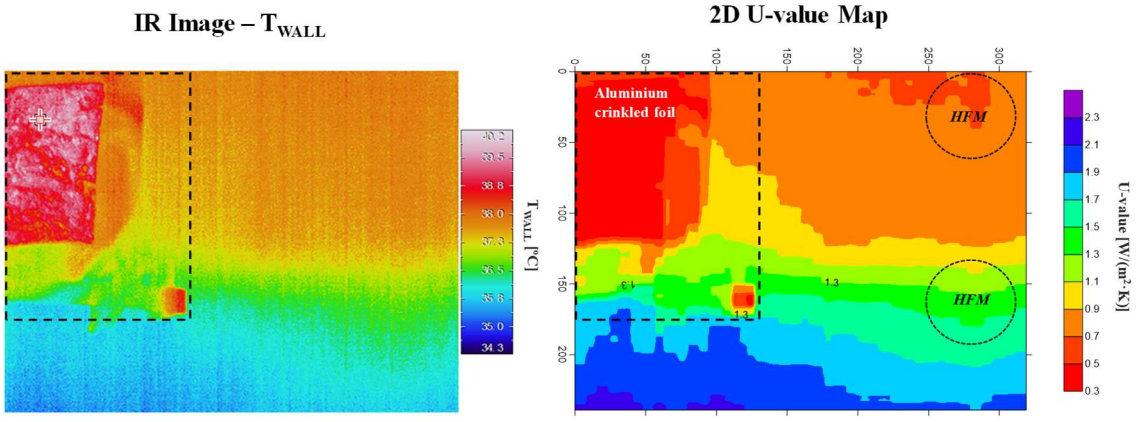

Figure 9. IR Image and 2D U-value map for the multi-leaf wall with internal horizontal thermal bridge (W3)

Generally speaking, all 2D contour maps were a great reproduction of the thermograms, since the parts with a higher proportion of mortar as well as anomalies of different depth or geometry were perfectly identified. For W1, it could be affirmed that the existence of air voids in the internal structure of the brick comprised the thermal behavior of the building component (Figure 7). For W2, the automated process allowed an easy interpretation of the thermal behaviour of each hole (Figure 8). In fact, it could be extrapolated that any significant deviation was detected for depths under 0.025 m, since the measured U-value inside the hole was practically equal to the surroundings. For W3, the automated process provided a completely identification of the internal cavity as well as its area of impact, which highlighted the distribution of thermal transmittance throughout the entire wall area (Figure 9). This aspect would be quite impossible with other NDT, since the common standardized methods (i.e. HFM) only provide local measurements. With this innovative tool, the technician could observe where the sample had intense fronts that urgently required solutions.

Regarding the reliability and quality of the automated process, readings of the 2D contour map were compared with HFM measurements. A brief description is reported below. In the case of W1 (Figure 7), the central area of the bricks of W1 had a U-value measured by QIRT similar to the outcomes obtained by HFM: $U_{QIRT\ map}$ = 1.1 -1.3 W/m^2·K in the map; U_{HFM_W1}= 1.308 W/(m^2·K) with SD= 0.683 W/(m^2·K). Notably, the internal thermal bridge and the borderlines among bricks could lead to variations in the thermophysical property above 53% ($U_{QIRT\ map}$ = 2 – 2.5 W/m^2·K). The second case study W2 (Figure 8) presented an alteration of 47% in the bottom of the wall area ($U_{QIRT\ map}$ = 0.4-0.8 W/m^2·K). For depths under 0.025 m, the U-value measured inside the hole was practically equal to the reference values. Thermal transmittance only fluctuated in the borderlines of the hole. For depths of 0.050 m, the thermal transmittance was found to be 0.4 W/m^2·K in the delimitation of the superficial thermal bridge and 1- 1.2 W/m^2·K in the central area of the anomaly. For depths of 0.065 m, the impact of the defect could derive to an increase in the U-value up to 10 times higher. As concerns normal operative conditions, the thermal transmittance was equal to 0.297 W/(m^2·K) with SD= 0.058 W/(m^2·K) using HFM. This value was within the range of the 2D map that was from 0.2 to 0.4 W/m^2·K. Finally, the readings of automated process for the case study W3 (Figure 9) were also in line with the HFM measurements. On the top of the thermogram and away from the horizontal TB, the thermal transmittance fluctuated between 0.3 - 0.5 W/m^2·K, which was really similar to the HFM readings (U_{HFM_W3}= 0.397 W/(m^2·K) with SD= 0.086 W/(m^2·K)). Nevertheless, values between

0.7 and 0.9 W/m^2·K were given for the main area without a thermal bridge. In the disturbed area, the impact of the internal cavity leads to $U_{HFM\_W3\ TB}$= 1.102 W/(m^2·K) with SD= 0.188 W/(m^2·K), which was within the range of the 2D map (0.9 - 1.3 W/m^2·K in the contour line).

Table 2 shows a comparative analysis of the common quantitative IRT strategies for homogenous and heterogeneous walls. Until now, an improvement in the inspection from inside the building was developed for homogeneous walls with different internal configurations, assuming instantaneous measured U-values as a stochastic process constituted by a constant signal plus white noise [Tejedor et al., 2019]. This aspect was an advantage in terms of automated inspection, since 30 minutes could be enough to assess homogenous heavy walls. In the current research, the potential of computing a 2D U-value map enhances the post-processing stage during quantitative IRT assessments for non-homogeneous walls in terms of complexity and time consumption. As seen in the above section, each IRT test can involve from 4 to 76800 elements to subdivide a thermal image, and this can imply more or less complexity of data management during the calculation procedure to determine the U-value. Concerning time consumption, it could be expressed as the sum of the sampling duration (time needed to perform the inspection) and the time required to draw up the data-processing (Equation 6). According to previous studies and Table 2, test duration is set from 120 to 180 minutes for heterogeneous walls, while $t_{data\text{-}processing}$ is found to be 3 hours per specific wall area or individual point without a 2D map.

$$Time\ consumption\ of\ QIRT = t_{INSPECTION} + t_{DATA\ PROCESSING} \quad (6)$$

According to UNE EN 1934:1998 [International Organization of Standardization, 1998] and Lucchi et al. [2018], an experimental procedure for inhomogeneous specimens should contain between 21 and 35 sensors to determine parameters such as the heat flux and wall surface temperatures at different points. However, from 6 to 30% of the measurement errors could be attributed to the features of sensors (i.e. size and location of the heat flux plate) [Meng et al., 2015; Cucumo et al., 2018; Soares et al., 2019] and 20% to the data processing methods [Cesaratto et al., 2013; Evangelisti et al., 2018]. The mapping proposal means that in-depth analysis of a building enclosure can be undertaken for several points at the same time, compared to the usual local diagnosis of the wall (without a 2D map) that requires the collection of IRT data in several wall areas and under the influence of changing test conditions over time (Table 2). Therefore, the automated

process implies an increase in robustness of the QIRT as a non-invasive technique with an acceptable loss of image quality (6.65%) and a notably reduction of costs and measurement errors related to the sensor network, to certify the built quality in new buildings and to decide on refurbishment solutions for existing buildings. Within the European context, Spain and Portugal have similarities in terms of climate zones and less demanding requirements in the thermal transmittance [Bienvenido-Huertas et al., 2019b]. Most of Spanish residential buildings were built between 1940 and 1979 (before the first thermal regulation) [Kurtz et al., 2015; Gangolells et al., 2016] and the U-values are higher than the limit set by the Spanish Technical Building Code [Kurtz et al., 2015], exceeding >100% the maximum energy loss value of façades [Moyano Campos et al., 2017]. However, progressive degradation of buildings could also be attributed to the lack of building maintenance plans [Bienvenido-Huertas et al., 2019c]. Along this line, Fantozzi et al. [2019] mentioned that the improvement of façades, the effect of thermal bridges and air ventilation rate should be considered to achieve nZEB in mild climate countries. Taking into account that the refurbishment is one of the passive strategies for energy optimization and building protection in the Mediterranean and Atlantic climate [Serrano et al., 2015; Suárez et al., 2016; Moyano Campos et al., 2017; Bienvenido-Huertas et al., 2019b; Fantozzi et al., 2019], the 2D U-value map could help to check the level of maintenance and safety of the existing and new buildings. The degree of heterogeneity in the distribution of heat flux and wall surface temperature means that the technician must make a considerable effort if he or she wants to quantify thermal transmittance and incorporate more insulation in those damaged structures or increase tasks of preventive maintenance. With this automated process, technicians can work with a simpler processed image through short-lasting evaluation, since 20 minutes could be enough to generate the 2D U-value map.

488 Table 2. Potentialities of the 2D U-value map

Homogeneous walls (without 2D U-value map)	
Test duration by the usual QIRT approach (Stochastic process by Tejedor et al. [2019])	30 minutes with a data acquisition interval = 1 minute
Number of thermograms	30 thermograms for a specific wall surface area
Estimated time for data-processing	30 minutes for a specific wall surface area
Non-homogeneous walls (without 2D U-value map)	
Test duration by the usual QIRT approach	120 – 180 minutes with a data acquisition interval = 1 minute
Number of thermograms	Minimum 120 thermograms
Estimated time for data-processing	3 hours to analyse each wall surface area or spot with anomaly • The distribution of the U-value in the different regions influenced by a defect cannot be identified • The U-value needs to be known for the undisturbed area to be taken as a reference • To assess multiple areas, 76800 elements with different T_{WALL} should be computed • Additional measurement techniques (EC, ERM, ERT and GPR) or complex CFD simulations need to be implemented to quantify the impact of the anomalies
Non-homogeneous walls (with 2D U-value map)	
Test duration by the usual QIRT approach	120 – 180 minutes with a data acquisition interval = 1 minute
Number of thermograms	Minimum 120 thermograms
Estimated time for data-processing	20 minutes for an entire wall area • Distribution of the U-value in any point of the building material, regardless the degree of homogeneity • 1600 elements with different T_{WALL} • Acceptable loss of the quality image (6.65%) • Great reproduction of the original thermogram • Non additional techniques are required • Improvement of the robustness

489

490

491

5. CONCLUSIONS

The main contribution of this research is the development of a method to create 2D U-value map for entire façades in operating conditions by means of in-situ QIRT tests, leading to a better and accurate energy diagnosis tool without additional measurement techniques (i.e. EC, ERM, ERT and GPR) or simulation (i.e. FLUENT, THERM etc). The formulation of the in-situ measured thermal transmittance was based on a validated internal QIRT method that had been executed on the real built environment (existing and new buildings of Spain with different features) under stationary regime [Tejedor et al., 2017; Tejedor et al., 2018; Tejedor et al., 2019]. For this research, three common constructive solutions in Southern European countries were reproduced in a climatic chamber. In this way, it could be easier to detect errors in the computation process of the 2D U-value map, since the environmental conditions of the laboratory were monitored and controlled in real time. Hence, the current study is a proof concept that deserves further research in future.

The analysis of the impact of mesh discretization in the processed image allowed to determine the optimum number of elements in which to subdivide a thermal image through the 2D Correlation Coefficient. The results revealed that 1600 elements of 8x6 pixels should be considered to generate the processed image, assuming a loss of quality of the image of around 6%. Regarding the obtained 2D U-value maps, all of them successfully reproduced the original thermogram. The automated process shows a good reliability and quality, since the readings of the 2D U-value maps are in line with the HFM measurements. Hence, the innovative tool allows: (i) the provision of information about the thermal behaviour of opaque façades along the vertical and horizontal axis; (ii) the definition of the geometric shape of the building element and its anomalies; (iii) the reduction of the complexity and time consumption of the current methodologies in terms of data management, executing several points of analysis at the same time.

The findings of the comparative analysis between current calculation procedures and strategies during the data-processing stage demonstrated the effectiveness of automating thermographic assessments. The innovative tool took just 20 minutes to evaluate the 2D effect of any anomaly, for homogeneous and heterogeneous construction materials. Furthermore, it avoided the manual collection and evaluation of a greater number of local measurements in several wall areas and under the variations of boundary conditions over time.

In terms of applicability, this automated data-processing technique could help to better understand the thermal behaviour of the wall when some anomalies arise by ageing or climatic conditions. In contrast to previous studies focused on the automated interpretation of building pathologies, the 2D colour map allows to identify the distribution of the measured thermal transmittance instead of only giving the linear U-value or the contour of the candidate to be a thermal bridge or a moisture region. It neither requires additional visual image processing techniques (thresholding, filtering etc) nor statistical tools such as PCT. It should be noted that internal or external walls can present pathologies that damage the structure and influence on energy demand [Dowson et al., 2012; Battista et al., 2014; Kurtz et al., 2015; Dumitrescu et al., 2016; Mortarotti et al., 2017; Park et al., 2017; Garrido et al., 2018a]. Furthermore, construction project documents cannot be obtained in most cases because the information in paper disappeared [Tejedor et al., 2017] or properties of the wall (stratigraphy and modularity) are unknown [Doran 2001; Baker et al., 2011; Litti et al., 2015; Lucchi et al., 2018] and consequently, an energy audit could imply a high cost in terms of money and time [Garrido et al., 2018a]. This research pretends to offer a fast, economic and easy tool for specialized researchers, energy auditors or other stakeholders related to construction field (civil engineers, industrial engineers or architects). In Southern European countries, where the residential building stock is characterized by being erected between 1940 and 1979 and having less demanding thermal requirements [Kurtz et al., 2015; Gangolells et al., 2016], refurbishment is presented as one of the passive strategies for optimizing energy use and building protection [Serrano et al., 2015; Suárez et al., 2016; Moyano Campos et al., 2017; Bienvenido-Huertas et al., 2019b; Fantozzi et al., 2019]. Therefore, the 2D U-value map could be a useful building diagnosis tool in the improvement of the façade as well as the design of preventive maintenance and safety plans. In the same way, and regarding the historic preservation, mapping the building's conservation state could help to define specific strategies to enhance the weaknesses of the structure.

Concerning the robustness of the equipment, this proposed tool leads to reduce the cost and measurement errors related to the sensor network. The number of sensors for heterogeneous walls is only 3 with the 2D U-value map (IR camera and two thermocouples) in comparison with regulations or previous studies where the metering section required a maximum of 35 sensors [UNE EN 1934:1998 - International Organization of Standardization, 1998-; Lucchi et al., 2017]. As mentioned in the literature, the subjectivity and expertise of the technician can play an important role in the correct identification of building pathologies [Garrido et

552 al., 2018]. Hence, human errors or procedural flows could be eliminated as a root-cause of inaccuracy if
553 the 2D-value map is used. The execution of the QIRT from inside the building also makes possible to avoid
554 the distortions of the thermograms caused by the lens of the IR camera. As regards, the integration of the
555 2D U-value map into digital tools, future steps of the research should involve a unique platform where all
556 softwares interact with each other (i.e. FLIR TOOLS+ or InfRec Analyser, MATLAB and SURFER).
557
558 **CONFLICT OF INTEREST**
559 The authors have no conflict of interest
560
561 **ACKNOWLEDGEMENTS**
562 This work was financially supported by: UID/ECI/04708/2019 - CONSTRUCT - Instituto de I&D em
563 Estruturas e Construções funded by national funds through the FCT/MCTES (PIDDAC)
564
565 **REFERENCES**
566 [1] Adhikari, R; Lucchi, E; Pracchi, V. *Experimental measurements on thermal transmittance of the opaque*
567 *vertical walls in the historical buildings*. Proceedings of PLEA2012 International Conference on Passive
568 and Low Energy Architecture, Lima, Peru, 2012. ISBN 9786124057892. https://www.researchgate.net/
569 publication/282337875_Experimental_Measurements_on_Thermal_Transmittance_of_the_Opaque_Verti
570 cal_Walls_in_the_Historical_Buildings [Accessed date: 20 December 2019]
571
572 [2] Bienvenido-Huertas, D; Moyano, J; Marín, D; Fresco-Contreras, R. *Review of in-situ methods for*
573 *assessing the thermal transmittance of walls*. Renewable and Sustainable Energy Reviews 102 (2019) pp.
574 356 – 371 https://doi.org/10.1016/j.rser.2018.12.016
575
576 [3] Dowson, M; Poole, A; Harrison, D; Susman, G. *Domestic UK retrofit challenge: barriers, incentives*
577 *and current performance leading into the Green Dale*. Energy Policy 50 (2012) pp. 294 – 305
578 https://doi.org/10.1016/j.enpol.2012.07.019
579

[4] Battista, G; Evangelisti, L; Guattari, C; Basilicata, C; De Lieto, R. *Buildings energy efficiency: interventions analysis under a smart cities approach*. Sustainability 6 (2014) pp. 4694 – 4705 https://doi.org/10.3390/su6084694

[5] Kurtz, F; Monzón, M; López –Mesa, B. *Energy and acoustics related obsolescence of social housing of Spain's post-war in less favored urban areas. The case of Zaragoza*. Informes de la Construcción, 67 (EXTRA-1): m021. http://dx.doi.org/10.3989/ic.14.062 [Accessed date: 20 December 2019]

[6] Mortarotti, G; Morganti, M; Cecere, C. *Thermal analysis and energy-efficient solutions to preserve listed building façades: the INA –Casa building heritage*. Buildings 7 (2017) pp. 1 – 22 https://doi.org/10.3390/buildings7030056

[7] Park, K; Kim, M. *Energy demand reduction in the residential building sector: A case study of Korea*. Energies 10 (2017) pp. 1 – 11 https://doi.org/10.3390/en10101506

[8] Ferrari, S; Zanotto, V. *The thermal performance of walls under actual service conditions: Evaluating the results of climatic chamber tests*. Construction and Building Materials 43 (2013) pp. 309-316 https://doi.org/10.1016/j.conbuildmat.2013.02.056

[9] Nardi, I; Sfarra, S; Ambrosini, D. *Quantitative thermography for the estimation of the U-Value: state of art and a case study*. 32nd IUT (Italian Union of Thermo-fluid-dynamics) Heat Transfer Conference, Journal of Physics, Conference Series 547 (2014) 012016 https://www.researchgate.net/publication/268508813_Quantitative_thermography_for_the_estimation_of_the_U-value_State_of_the_art_and_a_case_study [Accessed date: 20 December 2019]

[10] Soares, N.; Martins, C; Gonçalves, M; Santos, P; Simões da Silva, L; Costa, J.J. *Laboratory and in-situ non-destructive methods to evaluate the thermal transmittance and behaviour of walls, windows and construction elements with innovative materials: A review*. Energy and Buildings 182 (2019) pp. 88 – 110 https://doi.org/10.1016/j.enbuild.2018.10.021

610 [11] Peng, C; Wu, Z. *In situ measuring and evaluating the thermal resistance of building construction*.
611 Energy and Buildings 40 (2008) pp. 2076-2082 https://doi.org/10.1016/j.enbuild.2008.05.012
612
613 [12] Melo, A.P; Barcelos, M.M; Folle, D. *Análise térmica e energética da aplicação de isolante térmico*
614 *em fachadas e cobertura de um edificio comercial*. Revista de engenharia civil IMED 2 (2015) pp. 40 – 49.
615 ISSN 2358-6508 http://dx.doi.org/10.18256/2358-6508/rec-imed.v2n1p40-49 [Accessed date: 20
616 December 2019]
617
618 [13] Garrido, I; Lagüela, S; Arias, P; Balado, J. *Thermal-based analysis for the automatic detection and*
619 *characterization of thermal bridges*. Energy and Buildings 158 (2018a) pp. 1358 – 1367
620 https://doi.org/10.1016/j.enbuild.2017.11.031
621
622 [14] Avedilidis, N.P; Moropouloou, A. *Application of infrared thermography for the investigation of*
623 *historic structures*. Journal of Cultural Heritage 5 (2000) pp. 119 – 127 https://doi.org/10.1016/j.culher.
624 2003.07.002
625
626 [15] Moropoulou, A; Labropoulos, K.C; Delegou, E.T; Karoglou, M; Bakolas, A. *Non-destructive*
627 *techniques as a tool for the protection of built cultural heriatge*. Construction and Building Materials 48
628 (2013) pp. 1222 – 1239 https://doi.org/10.1016/j.conbuildmat.2013.03.044
629
630 [16] Stimolo, M. *Bridge and road construction. Passive infrared thermography: an inspection and*
631 *observation tool in bridge and road construction*. International Symposium (NDT-CE-2003), Non-
632 Destructive Testing in Civil Engineering, 2003. https://www.ndt.net/article/ndtce03/papers/v083/v083.htm
633 [Accessed date: 20 December 2019]
634
635 [17] Bashkar, S; Srinivasan, P; Chellapan, A. *Condition assessment of 30 years old overhead RCC*
636 *reservoir*. Proc. National Seminar on Non-Destructive Evaluation, December 7-9 2006, Hyderabad, India.
637 https://www.ndt.net/article/nde-india2006/files/tp-12-pap.pdf [Accessed date: 20 December 2019]
638

639 [18] Sassine, E. *A practical method for in-situ thermal characterization of walls*. Case Studies in Thermal
640 Engineering 8 (2016) pp. 84 – 93 https://doi.org/10.1016/j.csite.2016.03.006
641
642 [19] Tejedor, B; Casals, M; Gangolells, M. *Assessing the influence of operating conditions and*
643 *thermophysical properties on the accuracy of in-situ measured U-values using quantitative internal*
644 *infrared thermography*. Energy and Buildings 171 (2018) pp. 64 – 75 https://doi.org/10.1016/j.enbuild.
645 2018.04.011
646
647 [20] Dumitrescu, L; Baran, I; Pescaru, R.A. *The influence of thermal bridges in the process of buildings*
648 *thermal rehanilitation*. Procedia Engineering 181 (2017) pp. 682-689
649 https://doi.org/10.1016/j.proeng.2017.02.450
650
651 [21] Doran, S. *Field of investigations of the thermal performance of constructions elements as built*. Report
652 No.78132. 2000 https://www.researchgate.net/publication/277854674_Field_Investigations_of_the_
653 thermal_performance_of_construction_elements_as_built [Accessed date: 20 December 2019]
654
655 [22] Baker, P. *Research into the thermal performance of traditional brick walls*. English Heritage, 2013,
656 Research Report 2: Thermal conductivities of three traditional bricks.
657 https://research.historicengland.org.uk/Report.aspx?i=15741 [Accessed date: 20 December 2019]
658
659 [23] Lucchi, E. *Thermal transmittance of historical stone masonries: A comparison among standard,*
660 *calculated and measured data*. Energy and Buildings 151 (2017) pp. 393 - 405
661 https://doi.org/10.1016/j.enbuild.2017.07.002
662
663 [24] Genova, E; Fatta, G. *The thermal performances of historic masonry: in-situ measurements of thermal*
664 *conductance on calcarenite stone walls in Palermo*. Energy and Buildings 168 (2018) pp. 363 – 373
665 https://doi.org/10.1016/j.egypro.2017.07.431
666

667 [25] Park, M-W; Brilakis, I. *Continuous localization of construction workers via integration of detection*
668 *and tracking*. Automation in Construction 72 (2016) pp. 129 – 142
669 https://doi.org/10.1016/j.autcon.2016.08.039
670
671 [26] Kropp, C; Koch, C; König, M. *Interior construction state recognition with 4D BIM registered image*
672 *sequences*. Automation in Construction 86 (2018) pp. 11 – 32 https://doi.org/10.1016/j.autcon.2017.10.027
673
674 [27] Asdrubali, F; Baldinelli, G; Bianchi, F. *A quantitative methodology to evaluate thermal bridges in*
675 *buildings*. Applied Energy 97 (2012) pp. 365 – 373 https://doi.org/10.1016/j.apenergy.2011.12.054
676
677 [28] Nardi, I; Lucchi, E; De Rubeis, T; Ambrosini, D. *Quantification of heat energy losses through the*
678 *building envelope: A state-of-the-art with critical and comprehensive review on infrared thermography*.
679 Building and Environment 146 (2018) pp. 190 – 205 https://doi.org/10.1016/j.buildenv.2018.09.050
680
681 [29] Cereijo, J; Lagüela, S; Roca, D; Martínez, J; Lorenzo, H. *Automatic detection of thermal bridges in*
682 *thermographic building inspections*. 40th IAHS World Congress on Housing. Sustainable Housing
683 Construction. December 2014, Funchal, Portugal https://www.researchgate.net/publication/335240713_
684 Automatic_Detection_of_Thermal_Bridges_in_Thermographic_Building_Inspections [Accessed date: 03
685 June 2020]
686
687 [30] Edis, E; Flores-Colen, I; De Brito, J. *Quasi-quantitative infrared thermographic detection of moisture*
688 *variation in façades with adhered ceramic cladding using principal component analysis*. Building and
689 Environment 94 (2015) pp. 97 – 108 https://doi.org/10.1016/J.BUILDENV.2015.07.027
690
691 [31] Cadelano, G; Bison, P; Bortolini, A; Ferrarini, G; Perano, F; Girotto, M; Volinia, M. *Monitoring of*
692 *historical frescoes by timed infrared imaging analysis*. Opto-Electronics Reviews 23 (2015) pp. 102 – 108
693 https://doi.org/10.1515/oere-2015-0012
694

695 [32] Georgescu, M.S; Ochinciuc, C.V; Georgescu, E.S; Colda, I. *Heritage and Climate Changes in*
696 *Romania: The St. Nicholas Church of Densus, from Degradation to Restoration*. Energy Procedia 133
697 (2017) pp. 76 – 85 https://doi.org/10.1016/j.egypro.2017.09.374
698
699 [33] Asdrubali, F; Baldinelli, G; Bianchi, F; Costarelli, D; Rotili, A; Seracini, M; Vinti, G. *Detection of*
700 *thermal bridges from thermographic images by means of image processing aproximation algorithms*.
701 Applied Mathematics and Computation 317 (2018) pp. 160 – 171
702 https://doi.org/10.1016/j.amc.2017.08.058
703
704 [34] Martínez-Garrido, M.I.; Fort, R; Gómez-Heras, M; Valles-Iriso, J; Varas-Muriel, M.J. *A*
705 *comprehensive study for moisture control in cultural heritage using non-destructive techniques*. Journal of
706 Applied Geophysics 155 (2018) pp. 36 – 52 https://doi.org/10.1016/j.jappgeo.2018.03.008
707
708 [35] Garrido, I; Lagüela, S; Arias, P. *Autonomous thermography: towards the automatic detection and*
709 *classification of building pathologies*. 14th Quantitative Infrared Thermography Conference (2018b).
710 https://www.researchgate.net/publication/326112389_Autonomous_thermography_towards_the_automati
711 c_detection_and_classification_of_building_pathologies [Accessed date: 20 December 2019]
712
713 [36] Garrido, I; Lagüela, S; Sfarra, S; Madruga, F.J; Arias, P. *Automatic detection of moistures in different*
714 *construction materials from thermographic images*. Journal of Thermal Analysis and Calorimetry 138
715 (2019a) pp. 1649 – 1668 https://doi.org/10.1007/s10973-019-08264-y
716
717 [37] Garrido, I; Lagüela, S; Sfarra, S; Solla, M. *Algorithms for the automatic detection and characterization*
718 *of pathologies in heritage elements from thermographic images*. The International Archives of the
719 Photogrammetry, Remote Sensing and Spatial Information Sciences, Volume XLII-2/W15. 27th CIPA
720 International Symposium "Documenting the past for a better future", 1-5 September 2019, Avila, Spain.
721 https://doi.org/10.5194/isprs-archives-XLII-2-W15-497-2019 [Accessed date: 20 December 2019]
722

723 [38] Ruiz –Valero, L; Flores Sasso, V; Prieto Vicioso, E. *In situ assessment of superficial moisture*
724 *condition in façades of historic building using non-destructive techniques*. Case Studies in Construction
725 Materials 10 (2019) e00228 https://doi.org/10.1016/j.cscm.2019.e00228
726
727 [39] Golden Software, 2018. SURFER. https://www.goldensoftware.com/products/surfer [Accessed date:
728 2 July 2019]
729
730 [40] William, G.F. *Historic building façades: the manual for maintenance and rehabilitation*. New York
731 Landmarks Conservancy, New York, 1997. ISBN-13: 978-0471144151
732
733 [41] Jukka, V. *Methods and instrumentation for measuring moisture in building structures.* Series E:
734 Electronic Publication E7, Helsinki University of Technology. Applied Electronics Laboratory, Finland,
735 2005. ISBN 951-22-7523-6
736
737 [42] Göller, A. *Multilayer microwave moisture scans at large areas in civil engineering*. Non-Destructive
738 Testing of Materials and Structures. Proceedings of NDTMS-2011 (2013) pp. 793 – 798.
739 https://doi.org/10.1007/978-94-007-0723-8_113
740
741 [43] Martin, K; Escudero, C; Erkoreka, A; Flores, L; Sala, J.M. *Equivalent wall method for dynamic*
742 *characterization of thermal bridges*. Energy and Buildings 55 (2012) pp. 704 – 714
743 https://doi.org/10.1016/j.enbuild.2012.08.024
744
745 [44] Nardi, I; Paoletti, D; Ambrosini, D; De Rubeis, T; Sfarra, S. *Validation of quantitative IR*
746 *thermography for estimating the U-value by a hot box apparatus*. Journal of Physics Conference 655 (2015)
747 https://doi.org/10.1088/1742-6596/655/1/012006
748
749 [45] O'Grady, A.M.; Lechowska, A.A; Harte, A.M. *Quantification of heat losses through building envelope*
750 *thermal bridges influenced by wind velocity using the outdoor infrared thermography technique*. Applied
751 Energy 108 (2017) pp. 1038 – 1052 https://doi.org/10.1016/j.apenergy.2017.09.047
752

[46] Baldinelli, G; Bianchi, F; Rotili, A; Costarelli, D; Seracini, M; Vinti, G; Asdrubali, F; Evangelisti, L. *A model for improvement of thermal bridges quantitative assessment by infrared thermography*. Applied Energy 221 (2018) pp. 854-864 https://doi.org/10.1016/j.apenergy.2017.11.091

[47] O'Grady, A.M.; Lechowska, A.A.; Harte, A.M. *Application of infrared thermography technique to the thermal assessment of multiple thermal bridges and windows*. Energy and Buildings 168 (2018) pp. 347 – 362 https://doi.org/10.1016/j.enbuild.2018.03.034

[48] Sfarra, S; Cicone, A; Yousefi, B; Ibarra-Castanedo, C; Perilli, S; Maldague, X. *Improving the detection of thermal bridges in buildings via on-site infrared thermography: The potentialities of innovative mathematical tools*. Energy and Buildings 182 (2019) pp. 159 – 171 https://doi.org/10.1016/j.enbuild.2018.10.017

[49] Zhang, L; Koch, R. *An efficient and robust line segment matching approach based on LBD descriptor and pairwise geometric consistency*. Journal of Visual Communication and Image Representation 24 (2013) pp. 794 – 805 https://doi.org/10.1016/j.jvcir.2013.05.006

[50] Zhao, C; Zhao, H. *Multimodal image matching based on multimodality robust line segment descriptor*. Neurocomputing 177 (2016) pp. 290 – 303 https://doi.org/10.1016/j.neucom.2015.11.025

[51] Gao, Y; Roux, J.J; Teodosiu, C; Zhao, L.H. *Reduced linear state model of hollow block walls, validation using hot box measurements*. Energy and Buildings 36 (2004) pp. 1107 – 1115 https://doi.org/10.1016/j.enbuild.2004.03.008

[52] Sala, J.M; Urresti, A; Martín, K; Flores, I; Apaolaza, A. *Static and dynamic thermal characterization of a hollow brick wall: tests and numerical analysis*. Energy and Buildings 40 (2008) pp. 1513 – 1520 https://doi.org/10.1016/j.enbuild.2008.02.011

781 [53] Lucchi, E; Roberti, F; Alexandra, T. *Definition of an experimental procedure with the hot box method*
782 *for the thermal performance evaluation of inhomogeneous walls*. Energy and Buildings 179 (2018) pp. 99-
783 111 https://doi.org/10.1016/j.enbuild.2018.08.049
784
785 [54] Wróbel, A; Kisilewickz, T. *Detection of thermal bridges: aims, possibilities and conditions*.
786 Proceedings of the 9th International Conference on quantitative infrared thermography, Technical
787 University of Lodz, Krakow (2008), pp. 45 – 67 https://www.researchgate.net/publication/305193558_
788 Thermographic_detection_of_thermal_bridges_-_aims_possibilities_and_conditions [Accessed date: 03
789 June 2020]
790
791 [55] Lehman, B; Ghazi Wakili, K; Frank, Th; Vera Collado, B; Tanner, Ch. *Effects of individual climatic*
792 *parameters on the infrared thermography of buildings*. Applied Energy 110 (2013) pp. 29-43
793 https://doi.org/10.1016/j.apenergy.2013.03.066
794
795 [56] Hiasa, S; Birgul, R; Necati Catbas, F. *A data processing methodology for infrared thermography*
796 *images of concrete bridges*. Computers and Structures 190 (2017) pp. 205 – 218
797 https://doi.org/10.1016/j.compstruc.2017.05.011
798
799 [57] Hoyano, A; Asano, K; Kanamaru, T. *Analysis of the heat flux from the exterior surface of buildings*
800 *using time sequential thermography*. Atmospheric Environment 33 (1999) pp. 3941 – 3951
801 https://doi.org/10.1016/S1352-2310(99)00136-3
802
803 [58] Madding, R. *Finding R-values of stud frame constructed houses with IR thermography*. Proceedings
804 of InfraMation (2008) https://www.researchgate.net/publication/285737245_Finding_R-values_of_Stud-
805 Frame_Constructed_Houses_with_IR_Thermography [Accessed date: 20 December 2019]
806
807 [59] Albatici, R; Tonelli, A.M. *Infrared thermovision technique for the assessment of thermal transmittance*
808 *value of opaque building elements on site*. Energy and Buildings 42 (2010) pp. 2177 – 2183
809 https://doi.org/10.1016/j.enbuild.2010.07.010
810

811 [60] Fokaides, P.A.; Kalogirou, S.A. *Application of infrared thermography for the determination of the*
812 *overall heat transfer coefficient (U-Value) in building envelopes*. Applied Energy 88 (2011) pp. 4358 –
813 4365 https://doi.org/10.1016/j.apenergy.2011.05.014
814
815 [61] Dall'O, G; Sarto, L; Panza, A. *Infrared screening of residential buildings for energy audit purposes:*
816 *results of a field test*. Energies 6 (2013) pp. 3859 – 3878 https://doi.org/10.3390/en6083859
817
818 [62] Liu, J; Heidarinejad, M; Gracik, S; Srebric, J. *The impact of exterior surface convective heat transfer*
819 *coefficients on the building energy consumption in urban neighbourhoods with different plan area densities*.
820 Energy and Buildings 86 (2015) pp. 449 – 463 https://doi.org/10.1016/j.enbuild.2014.10.062
821
822 [63] Nardi, I; Paoletti, D; Ambrosini, D; de Rubeis, T; Sfarra, S. *U-Value assessment by infrared*
823 *thermography: A comparison of different calculation methods in a Guarded Hot Box*. Energy and Buildings
824 122 (2016) pp. 211-221 https://doi.org/10.1016/j.enbuild.2016.04.017
825
826 [64] Tejedor, B; Casals, M; Gangolells, M; Roca, X. *Quantitative internal infrared thermography for*
827 *determining in-situ thermal behaviour of façades*. Energy and Buildings 151 (2017) pp. 187 – 197
828 https://doi.org/10.1016/j.enbuild.2017.06.040
829
830 [65] Emmel, M.G; Abadie, M.O.; Mendes, N. *New external convective heat transfer coefficient correlations*
831 *for isolated low -rise buildings*. Energy and Buildings 39 (2007) pp. 335-342
832 https://doi.org/10.1016/j.enbuild.2006.08.001
833
834 [66] Palyvos, J.A. *A survey of wind convection coefficient correlations for building envelope energy*
835 *systems' modelling*. Applied Thermal Engineering 28 (2008) pp. 801-808
836 https://doi.org/10.1016/j.applthermaleng.2007.12.005
837
838 [67] Rabadiya, A.V.; Kirar, R. *Comparative analysis of wind loss coefficient (wind heat transfer coefficient)*
839 *for solar plate collector*. International Journal of Emerging Technology and Advanced Engineering

(IJETAE). ISSN 2250-2459, Volume 2, Issue 9, 2012 https://citeseerx.ist.psu.edu/viewdoc/download?doi=10.1.1.413.5300&rep=rep1&type=pdf [Accessed date: 20 December 2019]

[68] Sham, J.F.C; Lo, T.Y.; Memon, S.A. *Verification and application of continuous surface temperature monitoring technique for investigation of nocturnal sensible heat release characteristics by building fabrics.* Energy and Buildings 53 (2012) pp. 108-116 https://doi.org/10.1016/j.enbuild.2012.06.018

[69] Tejedor, B; Casals, M; Macarulla, M; Giretti, A. *U-value time series analyses: Evaluating the feasibility of in-situ short-lasting IRT tests for heavy multi-leaf walls*. Building and Environment 159 (2019) pp. 1 – 19 https://doi.org/10.1016/j.buildenv.2019.05.001

[70] Brilakis, I; Park, M.W. *Automated vision tracking of project related entities*. Advanced Engineering Informatics 25 (2011) pp. 713 – 724 https://doi.org/10.1016/j.aei.2011.01.003

[71] Montanini, R; Quattrocchi, A; Piccolo, S.A. *Active thermography and post-processing image enhancement for recovering of abraded and paint-covered alphanumeric identification*. Infrared Physics & Technology 78 (2016) pp. 24 – 30 https://doi.org/10.1016/j.infrared.2016.07.008

[72] Chrysafi, A.P; Athanasopoulos, N; Siakavellas, N.J. *Damage detection on composite materials with active thermography and digital image processing*. International Journal of Thermal Sciences 116 (2017) pp. 242 – 253 https://doi.org/10.1016/j.ijthermalsci.2017.02.017

[73] D'Accardi, E; Palumbo, E; Tamborrino, R; Galietti, U. *Quantitative analysis of thermographic data through different algorithms*. Procedia Structural Integrity 8 (2018) pp. 354 – 367 https://doi.org/10.1016/j.prostr.2017.12.036

[74] Kaur, A; Kaur, L; Gupta, S. *Image recognition using coefficient of correlation and structural similarity index in uncontrolled environment*. International Journal of Computer Application 59 (2012) pp. 0975 – 8887 https://doi.org/10.5120/9546-3999

[75] Blaber, J; Adair, B; Antoniou, A. *Ncorr: Open-Source 2D Digital Image Correlation Matlab Software*. Experimental Mechanics 55 (2015) pp. 1105 – 1122. https://doi.org/10.1007/s11340-015-0009-1

[76] Mohapatra, S; Weisshaar, J.C. *Modified Pearson correlation coefficient for two-color imaging in spherocylindrical cells*. BMC Bioinforatics (2018) https://doi.org/10.1186/s12859-018-2444-3 [Accessed date: 20 December 2019]

[77] Sultan, A.A; Washer, G. *A pixel-by-pixel reliability analysis of infrared thermography (IRT) for the detection of subsurface delamination*. NDT and E International 92 (2017) pp. 177 -186 https://doi.org/10.1016/j.ndteint.2017.08.009

[78] Milovanovic, B. *Defect detection in concrete using principle component thermography*. International Conference on Sustainable Materials, Systems and Structures. SMSS 2019 Novel Methods for Characterization of Materials and Structures. March, 2019 https://www.researchgate.net/publication/331982138_Defect_detection_in_concrete_using_principle_component_thermography [Accessed date: 03 June 2020]

[79] González-Jorge, H; Lagüela, S; Krelling, P; Armesto, J; Martínez-Sánchez, J. *Single image rectification of thermal images for geometric studies in façade inspections*. Infrared Physics & Technology 55 (2012) pp. 421 – 426 https://doi.org/10.1016/j.infrared.2012.05.003

[80] MathWorks, 2018. MATLAB Software https://es.mathworks.com/ [Accessed date: 9 June 2019]

[81] International Organization for Standardization, 2014. *ISO 9869:2014 Thermal insulation. Building elements. In –situ measurement of thermal resistance and thermal transmittance. Part 1: Heat flow meter method* https://www.iso.org/standard/59697.html [Accessed date: 15 April 2019]

[82] Chen, F; Wiitkopf, S.K. *Summer condition thermal transmittance measurement of fenestration systems using calorimetric hot box*. Energy and Buildings 53 (2012) pp. 47 – 56 https://doi.org/10.1016/j.enbuild.2012.07.005

[83] International Organization for Standardization, 1998. *UNE EN 1934:1998 Thermal performance of buildings - Determination of thermal resistance by hot box method using heat flow meter – Masonry* https://www.en.aenor.com/normas-y-libros/buscador-de-normas/une?c=N0014601 [Accessed date: 15 April 2019]

[84] Meng, X; Yan, B; Gao, Y; Wang, J; Zhang, W; Long, E. *Factors affecting the in-situ measurement accuracy of the wall heat transfer coefficient using the heat flow meter method*. Energy and Buildings 86 (2015) pp. 754 – 765 https://doi.org/10.1016/j.enbuild.2014.11.005

[85] Cucumo, M; Ferraro, V; Kaliakatsos, D; Mele, M. *On the distortion of thermal flux and surface temperature induced by heat flux sensors positioned on the inner surface of buildings*. Energy and Buildings 158 (2018) pp. 677 – 683 https://doi.org/10.1016/j.enbuild.2017.10.034

[86] Cesaratto, P.G; De Carli, M. *A measuring campaign of thermal conductance in situ and possible impacts on net energy demand in buildings*. Energy and Buildings 59 (2013) pp. 29 – 36 https://doi.org/10.1016/j.enbuild.2012.08.036

[87] Evangelisti, L; Guattari, C; Asdrubali, F. *Influence of heating systems on thermal transmittance evaluations: simulations, experimental measurements and data-processing*. Energy and Buildings 168 (2018) pp. 180 – 190 https://doi.org/10.1016/j.enbuild.2018.03.032

[88] Bienvenido-Huertas, D; Oliveira, M; Rubio-Bullido, C; Marín, D. A *Comparative analysis of the international regulation of thermal properties in building envelope*. Sustainability 11 (2019b) 5574 https://doi.org/10.3390/su11205574

[89] Gangolells, M; Casals, M; Forcada, N; Macarulla, M; Cuerva, E. *Energy mapping of existing building stock in Spain*. Journal of Cleaner Production 112 (2016) pp. 3895 – 3905 https://doi.org/10.1016/j.jclepro.2015.05.105

929 [90] Moyano Campos, J.J; Antón García, D; Rico Delgado, F; Marín García, D. *Threshold values for energy*
930 *loss in building façades using infrared thermography*. Sustainable Development and Renovation in
931 Architecture, Urbanism and Enginneering. Springer International Publishing (2017) pp. 427 – 437
932 https://doi.org/10.1007/978-3-319-51442-0_35
933
934 [91] Bienvenido-Huertas, D; Rubio-Bellido, C; Sánchez-García, D; Moyano, J. *Internal Surface*
935 *condensation risk in façades of Spanish social dwellings.* Building Research & Information (2019c) pp.
936 928 – 947 https://doi.org/10.1080/09613218.2019.1612729
937
938 [92] Fantozzi, F; Hamdi, H; Rocca, M; Vegnuti, S. *Use of automated control systems and advanced energy*
939 *simulations in the design of climate responsive educational building for Mediterranean area*. Sustainability
940 11 (2019) 1160 https://doi.org/10.3390/su11061660
941
942 [93] Serrano Lanzarote, B; Sanchis Cuesta, A. *The technical inspection of buildings as an instrument for*
943 *the energy improvement of existing buildings*. Informes de la Construcción, Volumen 67, NT003 (2015).
944 ISSN-L: 0020 – 0883 http://dx.doi.org/10.3989/ic.14.052 [Accessed date: 03 June 2020]
945
946 [94] Suárez, R; Fragoso, J. *Passive strategies for energy optimization of social housing in the*
947 *Mediterranean Climate*. Informes de la Construcción, Volumen 68, e136 (2016). ISSN-L: 0020 – 0883
948 http://dx.doi.org/10.3989/ic.15.050 [Accessed date: 03 June 2020]
949
950 [95] Litti, G; Khosdel, S; Audenaert, A; Braet, J. *Hygrothermal performance evaluation of traditional brick*
951 *masonry in historic buildings*. Energy and Buildings 105 (2015) pp. 393 – 411
952 https://doi.org/10.1016/j.enbuild.2015.07.049
953